Finite Element Modelling of Nanostructured Piezoelectric Resonators (NAPIERs)

Joe E. A. Southin and Roger W. Whatmore, *Member, IEEE*

***Abstract*—A new modification to the traditional piezoelectric thin film bulk acoustic wave resonator (FBAR) and solidly mounted acoustic wave resonator (SMR) is proven to significantly improve their performances. The proposed design involves the surface micro/nano structuring of planar piezoelectric thin films to realize an array of a large number of rod-like structures. In contrast to the plate-like thickness extensional resonance in traditional FBAR and SMR devices, the rod-like structures can be excited in their length extensional resonance, yielding a higher electromechanical coupling factor and effectively eliminating the spurious resonances from lateral modes of vibration. The designs have been investigated by two and three-dimensional finite element analyses and one-dimensional transmission-line modelling. The results show that significant increases in the electromechanical coupling factor of ca. 40% can be achieved by using the rod-like length extensional resonances as compared with the plate-like thickness extensional resonances in traditional devices. Simulations show that rod width-to-thickness aspect ratios of less than 0.5 could result in an electromechanical coupling factor (k_{eff}^2) of over 10% for a zinc oxide device, compared with approximately 7% for a conventional design.**

I. Introduction

Significant study has been conducted in previous years on the behavior of piezoelectric resonating structures and devices by means of finite-element analyses (FEA). The drive toward systems miniaturization has been one of the major factors in the design of piezoelectric acoustic resonators, and finite-element modelling (FEM) has been shown to be a useful tool in the development and optimization of devices.

The work on 1-3 piezoelectric-polymer composites [1]–[5] has enabled the development of a new class of materials/devices with significantly increased piezoelectric coefficients (especially hydrostatic), now commonly used in underwater sonar applications and ultrasonic transducers. In these materials, an array of piezoelectric rods with one-dimensional (1D) inter-connectivity are encased in a polymer matrix of three-dimensional (3D) inter-connectivity.

The piezoelectric thin-film bulk acoustic resonator (FBAR) has been used widely as a frequency control device in wireless broadband communication systems due to its high quality factor, excellent stability against temperature variations, and demonstrated compatibility with integrated circuit processing. A layer of piezoelectric material is sandwiched between two metal electrode layers. AC electric fields in the thickness direction form longitudinal acoustic waves that propagate through the structure, causing the FBAR structure to resonate in the thickness-field-excitation mode. The sandwich structure is often supported on a membrane layer formed by bulk micromachining, as depicted in Fig. 1(a). Solidly mounted structures are also used whereby multiple impedance-transforming layers on a solid substrate acoustically isolate the piezoelectric layer from the substrate, often referred to as solidly mounted resonators, or SMR, as depicted in Fig. 1(b). In the latter design, a piezoelectric thin-film is deposited on top of a succession of quarter-wave-thick high and low acoustic impedance materials which act to acoustically isolate it from the substrate [6].

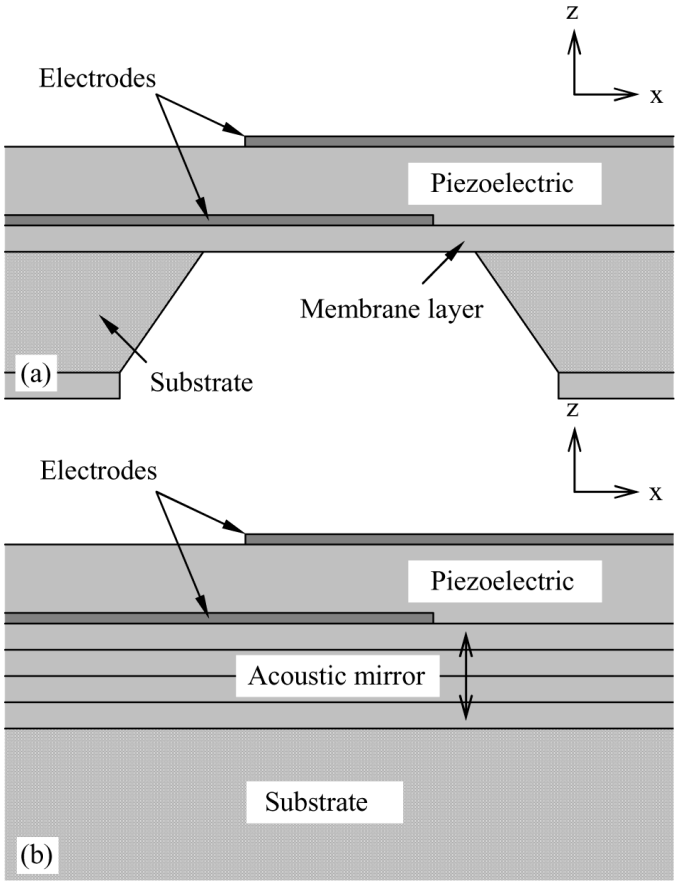

Fig. 1. Conventional design of a membrane-supported FBAR (a) and SMR (b).

FEM has been applied to a wide variety of micro-structured piezoelectric resonators, including the

Manuscript received May 15, 2003; accepted December 22, 2003.

The authors are with Cranfield University, Bedford, England, UK (e-mail: j.southin@cranfield.ac.uk).

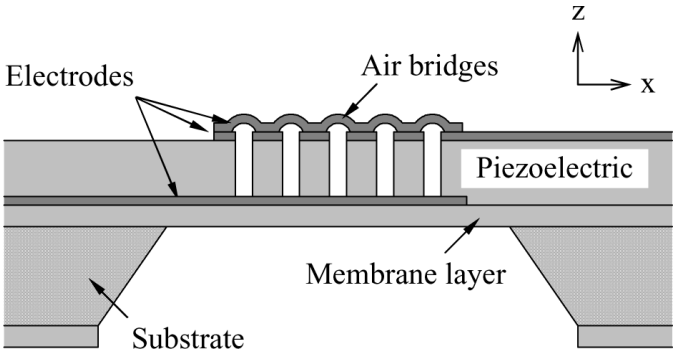

Fig. 2. Schematic illustration of the proposed NAnoscale PIEzoelectric Resonator (NAPIER) device. A piezoelectric thin-film is deposited on the substrate and is then structured into an array of rods. Top electrodes in the form of web-like interconnecting air bridges are required to electrically connect all rods in parallel.

membrane-FBAR and SMR structures. Some work has been conducted to further the understanding of the origins of spurious resonances in FBAR devices and other structures. Makkonen *et al.* showed FEM results successfully simulating the modes responsible for these spurious resonances [7], [8], and later confirmed their work by studies of the surface displacements for a variety of electrode shapes using laser probing [9], [10]. FEM studies by Kunkel *et al.* [11] of the resonance modes operating within piezoelectric resonant structures have provided data that explain the interaction between different resonance modes. The electromechanical coupling factors of different modes, mode interaction, and other topics are also covered by Lerch [12].

This paper describes a new modification to the traditional FBAR design that could significantly increase the electromechanical coupling factor and resonator Q-value, at the same time reducing the problematic spurious resonances associated with the plate-like thickness extensional resonance modes. This could be achieved by patterning the device on the nano-scale. The design consists of an array of rods resonating in parallel with one another, referred to as the NAnoscale PIEzoelectric Resonator (NAPIER) array, depicted schematically in Fig. 2. This contrasts with the more conventional design in which a planar piezoelectric layer undergoes thickness extensional resonance.

II. Methodology

For the purpose of the numerical modelling, three piezoelectric materials were selected for study: zinc oxide (ZnO), aluminium nitride (AlN), and lead zirconate titanate (PZT). Gold (Au) was chosen as both the top and the bottom electrode materials, and silicon (Si) was selected as the substrate material. For the membrane-FBAR models, the membrane material is silicon nitride (SiN_x). The acoustic reflector material pair for the SMR models are magnesium (Mg) and tungsten (W), with alternating layers of each. The final layer in contact with the silicon substrate is tungsten.

ANSYS version 5.7 (ANSYS, Inc., Canonsburg, PA) was used to perform the necessary 2-dimensional (2D) and 3D finite element simulations. The 3D simulations made use of the 8-node, hexahedral, linear, coupled-field element SOLID5 supplied in ANSYS for the piezoelectric materials and the 8-node, linear, structural element SOLID45 for the non-piezoelectric materials. In 2D simulations, 4-node quadrilateral linear coupled-field elements PLANE13 were used for the piezoelectric materials, employing the plane-strain option whereby the suppressed dimension is assumed to be infinite. The models were truncated at the edges of the membrane where fixed boundary conditions were applied in an approximation to the real device. The voltage degree of freedom on the nodes of each electrode were coupled together, implying ideal conduction, and voltage potentials of 0V and 1V were applied to the bottom and top electrodes, respectively.

Four different types of structures were investigated. First, a planar FBAR configuration was used to model the response of a traditional FBAR design. The second and third types of structures consisted of a piezoelectric block, either supported by a membrane layer or solidly mounted on a stack/tower of acoustic reflector layers on a substrate, referred to herein as the membrane-FBAR and columnar-SMR, respectively, Fig. 3(a) and (b). The fourth structure consisted of a piezoelectric block on planar acoustic reflector layers on a substrate, referred to herein as the planar-SMR, as depicted in Fig. 3(c). Periodic boundary conditions were applied to the latter three models to simulate the effects of an array of resonating blocks. The thickness of the ZnO piezoelectric layer was fixed at 1 μm and the widths of the blocks varied between 0.01 and 20 μm, in order to determine the effects of changing aspect ratio on the frequencies of the vibrational resonance modes. Both modal and harmonic analyses were run to characterize the behaviors of the finite-element models. Resistive and dielectric losses were not considered, as only mechanical losses could be included in coupled-field analyses in ANSYS version 5.7. In all models, a mechanical loss factor of 0.0012 was used.

The behaviors of the resonators were characterized in harmonic analyses by the electrical input impedance, calculated from the resultant nodal voltage V_i and charge Q_i on the top electrode according to $Z_i = V_i/I_i$, where $I_i = -2\pi i Q_i f = -i\omega Q_i$, and f is the frequency. The absolute value of the electrical input impedance was used to visualize the behavior of the resonators.

Both modal and harmonic analyses were employed to determine the resonance and anti-resonance frequencies for each vibrational mode of the piezoelectric resonator. For the modal analyses, short circuit (electrical voltage $\varphi = 0$) and open circuit (charge $Q_0 = 0$) resonance frequencies are obtained by solving the constitutive equations under the appropriate electrical boundary conditions. These correspond to the series resonance, f_s, and parallel resonance frequencies, f_p, respectively. A finite-element modal analysis determines the complete spectrum of series and parallel resonance frequencies in a certain frequency range but it is up to the user to pair the frequencies in sets that correspond to the underlying vibrational modes. Non-

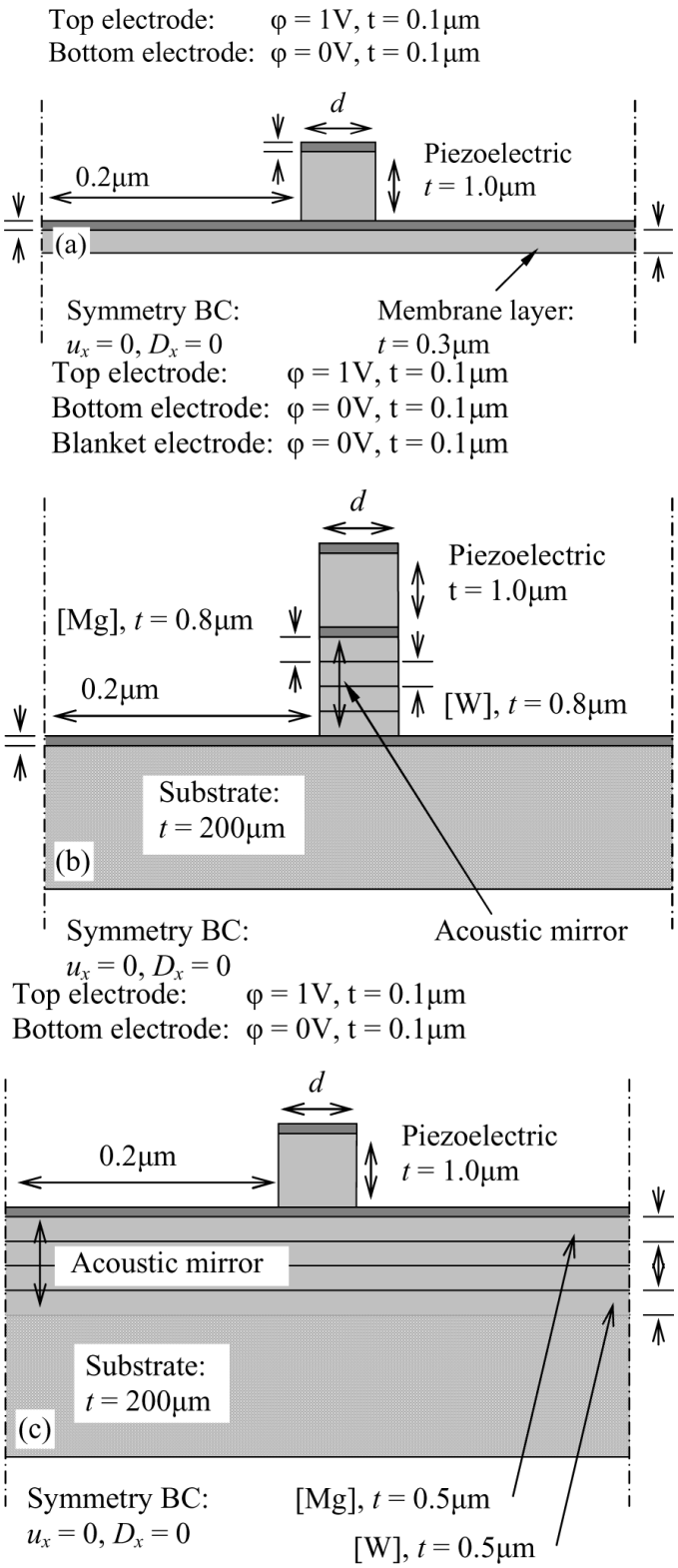

Fig. 3. Details of the finite-element model for (a) the nanostructured membrane-FBAR, (b) the nanostructured columnar-SMR, and (c) the nanostructured planar-SMR.

piezoelectric, or purely elastic, modes can be identified and eliminated immediately, because they have identical series and parallel resonance frequencies. For harmonic analyses, it is a valid assumption to use the frequencies of the minima and maxima in electrical input impedance as the resonance and anti-resonance frequencies, respectively, for a piezoelectric with a low loss. This method has the benefit of being able to visualize the frequency response of the piezoelectric resonator and so help to pair the correct resonance and anti-resonance frequencies, but at the cost of an increased computation time. Also, it is up to the user to locate any resonances in the impedance data, which reduces the number of modes that are identified.

For each vibrational resonance mode, the separation between the resonance and anti-resonance frequencies is indicative of the strength of the electromechanical coupling factor. An effective electromechanical coupling factor, k_{eff}, can be defined for a given mode [13]:

$$(k_{\text{eff}})^2 = \frac{\left(f_p^2 - f_s^2\right)}{f_p^2}, \tag{1}$$

where k_{eff} depends on both the material coupling factor and the resonator geometry, and so will be affected by varying the aspect ratio of the resonator device.

A semi-automated routine was prepared to carry out the modal analyses in order to determine the resonance and anti-resonance frequencies of piezoelectric blocks of varying aspect ratio. The series and parallel resonance frequencies of a 1-μm-thick piezoelectric block were determined as the width-to-thickness aspect ratio was increased from 0.01 to 10 μm in exponentially increasing intervals.

III. Resonator Modelling

When conducting finite element analyses, it is important to ensure that an appropriate mesh density has been chosen to guarantee accurate results. For acoustic devices, it is important that the mesh is sufficiently dense to enable the effects of travelling acoustic waves to be determined. An element size smaller than one-twentieth of the wavelength of the acoustic waves under study is preferred. Convergence testing of results with increasing mesh density implied that 10 mesh divisions through the thickness of the piezoelectric layer were sufficient. Due to the long computational time required to find solutions for the 3D models, it was decided to focus efforts on 2D analyses.

One of the difficulties associated with FEM of thin-film devices is the availability of appropriate material parameters, as thin-film values may vary considerably from bulk values. Although a vast amount of data exists on the material properties of piezoelectric thin-films in literature, relatively few address a complete characterization of any particular material. For many cases, the only alternative is to use bulk values and to be aware that the results from the subsequent FEA results may be affected as a result. The material parameters used for the numerical analyses de-

TABLE I
PIEZOELECTRIC MATERIAL PROPERTIES FOR ZNO THIN-FILM [14], MOTOROLA PZT 3203HD BULK CERAMIC [15], AND ALN THIN-FILM [16].

	ZnO	PZT	AIN	Units
ρ	5670	7850	3260	kg/m^3
c_{11}^E	207.0	143.4	345.0	GPa
c_{12}^E	117.7	92.9	125.0	GPa
c_{13}^E	106.1	102.9	120.0	GPa
c_{33}^E	209.5	142.5	395.0	GPa
c_{44}^E	44.8	25.5	118.0	GPa
c_{66}^E	44.65	25.3	110.0	GPa
e_{31}	−0.62	−11.67	−0.58	C/m^2
e_{33}	0.96	19.68	1.55	C/m^2
e_{24}	−0.37	14.23	−0.48	C/m^2
ε_{11}^S	8.33	1513	9.04	ε_0
ε_{33}^S	8.31	1301	10.73	ε_0

tailed here are shown in Table I for ZnO thin-film, a bulk PZT ceramic, and AlN thin-film.

IV. RESULTS

Comparisons of 2D and 3D data obtained by modal analyses to yield the resonance and anti-resonance frequencies of freely-suspended ZnO blocks have been shown to be consistent. The only differences observed were the omission of several modes of vibration in the 2D data, such as torsion modes, and a disagreement of the order of 15% for the predicted resonance frequencies in the extreme case of low-aspect-ratio rod-like models. Agreement between 2D and 3D data for plate-like models were typically $< 0.1\%$. Where accurate data were required for piezoelectric rods, full 3D analyses were used.

The results for the modal (series) resonance frequencies of freely-suspended piezoelectric blocks of varying aspect ratios for ZnO, PZT, and AlN are shown in Fig. 4(a)–(c). The rod-like extensional resonance mode can be seen in all three figures as the mode with the relatively flat response for lower aspect ratios. A series of "terraces" can also be seen in the figures for higher aspect ratios, indicating plate mode resonances such as the thickness-shear and thickness-extensional modes, consistent with the results of Kunkel *et al.* [11]. The anti-resonance (parallel) modal results appear very similar to those presented for the resonance (series) modes, and so are omitted here. It is possible to measure the separation between the resonance and anti-resonance frequencies, enabling a calculation of the effective electro-mechanical coupling factors through (1). The overall behavior of the different modes with varying aspect ratios is similar across the three different materials used, and the plate-like resonance and anti-resonance frequencies agree well with what is expected from theory (see Section V).

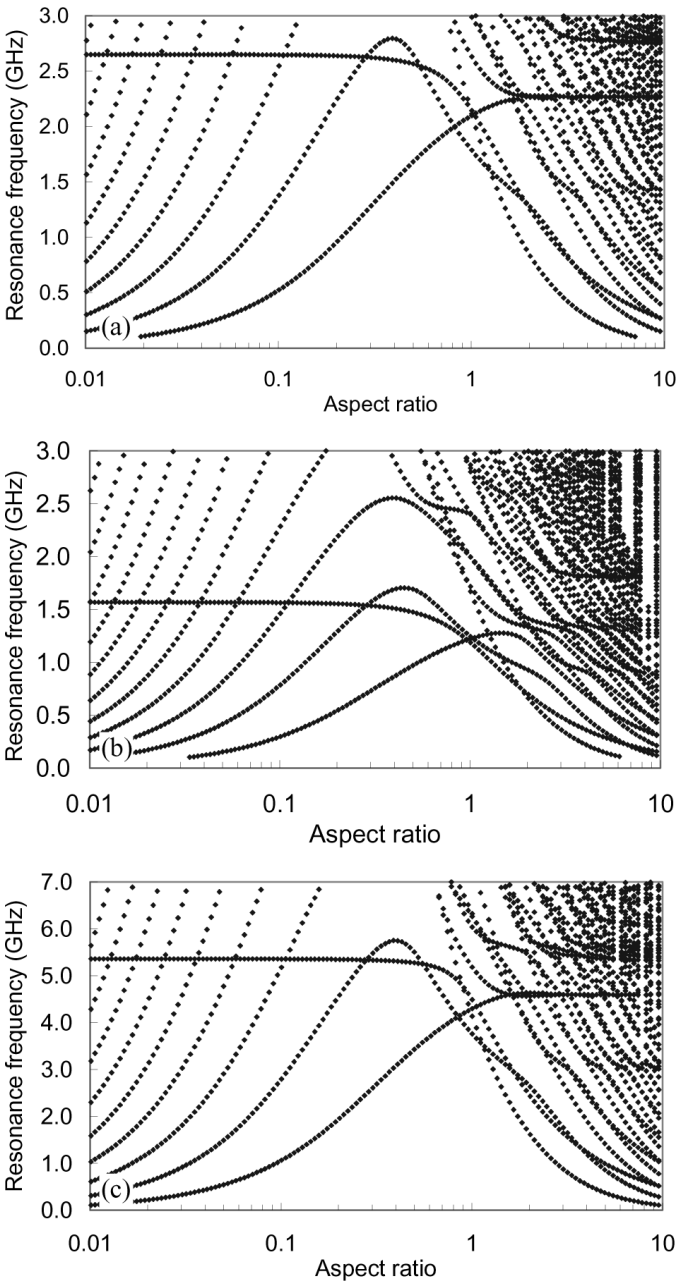

Fig. 4. Modal resonance frequencies as a function of aspect ratio for piezoelectric (a) ZnO, (b) PZT, and (c) AlN freely suspended blocks, as determined by 2D modal analyses.

A series of 2D plane-strain harmonic analyses of piezoelectric blocks were run using ZnO, PZT, and AlN as the piezoelectric material for comparison to the modal analyses results. The resonance and anti-resonance frequencies were recorded and paired where possible in order to calculate the effective electro-mechanical coupling factors of each mode as the piezoelectric block aspect ratios were varied. The effective electromechanical coupling factor results for ZnO, PZT, and AlN as calculated by harmonic analyses agreed well with the modal analysis results. The results for ZnO material are shown Fig. 5. The effects of including the electrode layers in the finite-element model can be seen in Fig. 5(b).

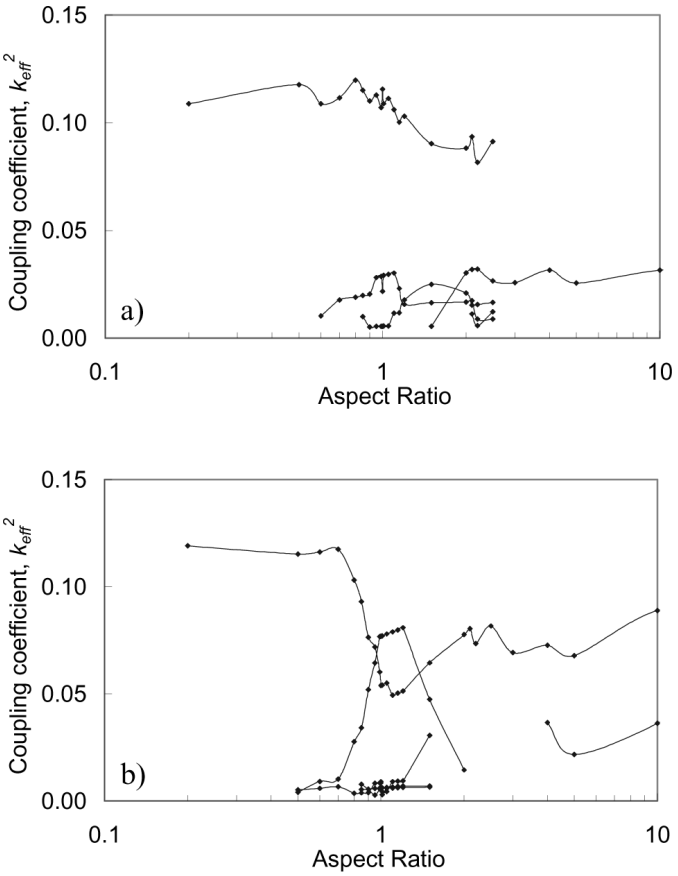

Fig. 5. Effective electromechanical coupling factors for the first few resonance modes in a freely suspended ZnO block of varying width-to-thickness aspect ratio (a) without electrodes and (b) with electrodes, as determined by 2D harmonic finite-element analyses.

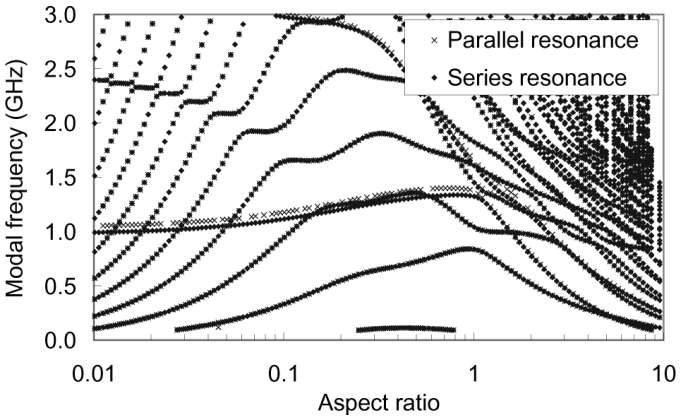

Fig. 6. Modal resonance and anti-resonance frequencies for a membrane-supported ZnO piezoelectric block as a function of aspect ratio, as determined by 2D modal analyses. Modes with high coupling factors can easily be identified as the modes which have an appreciable difference between the resonance and anti-resonance modal frequencies.

The mass-loading effects of the additional electrode layers are clearly visible in Fig. 5. The mode associated with the rod-like extension for the lower-aspect-ratio models can be attributed to the mode with the highest electromechanical coupling factor in each case, which has been verified by modal analyses. Slightly different behavior of the rod-like mode is noticed at lower frequencies, in that the modal frequencies tend to form a slight peak for aspect ratios at around unity, instead of forming a plateau at lower aspect ratios in the absence of electrode mass-loading. A large number of interacting modes of vibration clustered around the plate-like mode accounts for the "terrace" on the previous modal results. This makes it difficult to calculate the electromechanical coupling factor for the plate-like mode at higher aspect ratios from modal analyses alone as it becomes increasingly more difficult to pair the resonance and anti-resonance modes as the density of modes increases. The factor is easily calculated from harmonic analyses, with electromechanical coupling factors corresponding well to that expected from theory. The way in which different modes compete with one another in the electromechanical coupling factor results appears to be consistent with the results shown in Kunkel *et al.* [11]. What is immediately apparent is that the rod-like modes show a significant increase in the electromechanical coupling factor over the plate-like mode, suggesting an increased resonator performance may be possible by implementing rod-like resonances.

Limitations of using harmonic analyses in this way include the fact that pairing of resonance and anti-resonance still needs to be performed, and accuracy of the calculated coupling factors relies on the resolution of data points in the harmonic analyses. Well-separated modes are free from the former problems, but are still receptive to errors arising from the limited resolution of the harmonic analyses, as can be seen by the unsmooth variations in the coupling factor data for the highest coupling modes in Fig. 5. The errors in the lower coupling modes most probably arise from incorrect pairing of resonance and anti-resonance modes. As this method requires the data from each resonance mode to be manually extracted, only a subset of data is gathered leading to a greatly reduced density of data points as shown undulating in Fig. 5.

A. Membrane-Supported FBAR Structure

The modal method for determining resonance and anti-resonance frequencies was applied to the membrane-ZnO-FBAR structure, including the presence of Au electrodes 0.1 μm thick. Both the resonance and anti-resonance modal frequencies are shown in Fig. 6, and the effective electromechanical coupling factors for the two highest coupling modes are shown in Fig. 7. These results imply that a coupling factor of greater than 0.1 can be achieved for aspect ratios of less than 0.5, and a coupling factor of as much as 0.112 for aspect ratios less than 0.01. Interestingly, the second mode indicated in Fig. 7 peaks relatively sharply at an aspect ratio of approximately 1.5, also confirmed by harmonic analyses. It should be noted that full 3D analyses are required if accurate data are sought for piezoelectric rod-like structures. The shapes of these two modes have also been calculated by modal analyses and are also shown in Fig. 7 (inset). A second resonance mode

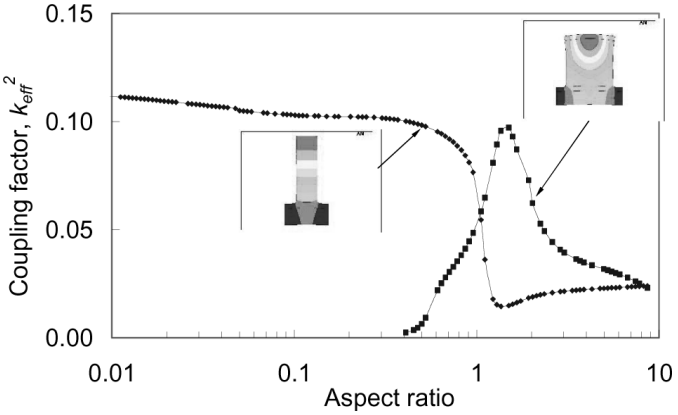

Fig. 7. Effective electromechanical coupling factors for the first two resonance modes in membrane-supported ZnO block (including electrode layers) as a function of aspect ratio, as determined by 2D modal analyses. Also displayed (inset) are the shapes of the two modes, showing contour plots of the vertical displacement field.

exists between f_p and f_s of the main resonance for a range of aspect ratios between 0.1 and 0.6, as shown in Fig. 6. This mode is not expected to degrade the performance of the main resonance as f_p and f_s are identical for this mode, indicating that it is a purely structural mode and not piezoelectric.

B. Solidly Mounted Resonators

One-dimensional analytical modelling of both the membrane-FBAR structure and the SMR structure was performed using the well-known transmission-line equation together with the analytical solution for a 1D slab of piezoelectric resonator. This 1D modelling approach was implemented using the software package MathCAD alongside finite-element analyses in ANSYS to aid the optimization process of the SMR acoustic reflector layers.

To demonstrate the performance of acoustically isolating layers in a planar-SMR model, three harmonic FEM simulations were run with 0 reflector layers, 1 pair of reflector layers, and 3 pairs of reflector layers. ZnO was chosen as the piezoelectric material, and all dimensions were as indicated in Fig. 4, with the exception that a planar ZnO layer was specified instead of a single block. The harmonic frequency response of electrical input impedance for the three cases are shown in Figs. 8(a)–(c).

The over-mode type resonances of the 200-μm-thick silicon cavity that couple to the fundamental thickness mode of the ZnO layer operating at approximately 1.8 GHz can clearly be seen. An increasing acoustic isolation can be achieved by adding larger numbers of acoustic reflector layers in between the piezoelectric layer and the substrate. A single clearly defined thickness resonance and acceptable acoustic isolation from the substrate can be achieved by three pairs of acoustic reflector layers in such a system, as illustrated in Fig. 8(c).

It is also possible to illustrate the behavior of the SMR structure using 1D analytical modelling. Lakin *et al.* [17] make reference to the concept of an acoustic reflector bandwidth that can be calculated by the 1D transmission-line model. The 1D analytical model was used to determine the frequency response of a 1-μm-thick ZnO resonator acoustically isolated from a 400-μm-thick silicon substrate by means of 10 pairs of magnesium and tungsten acoustic reflector layers, and the results showed that the acoustic reflector operates optimally for a range of frequencies in which the acoustic waves are confined to the piezoelectric resonating layer. By carefully considering operating frequency, material properties, and layer thicknesses, an appropriate acoustic reflector bandwidth can be tailored to suit a particular device.

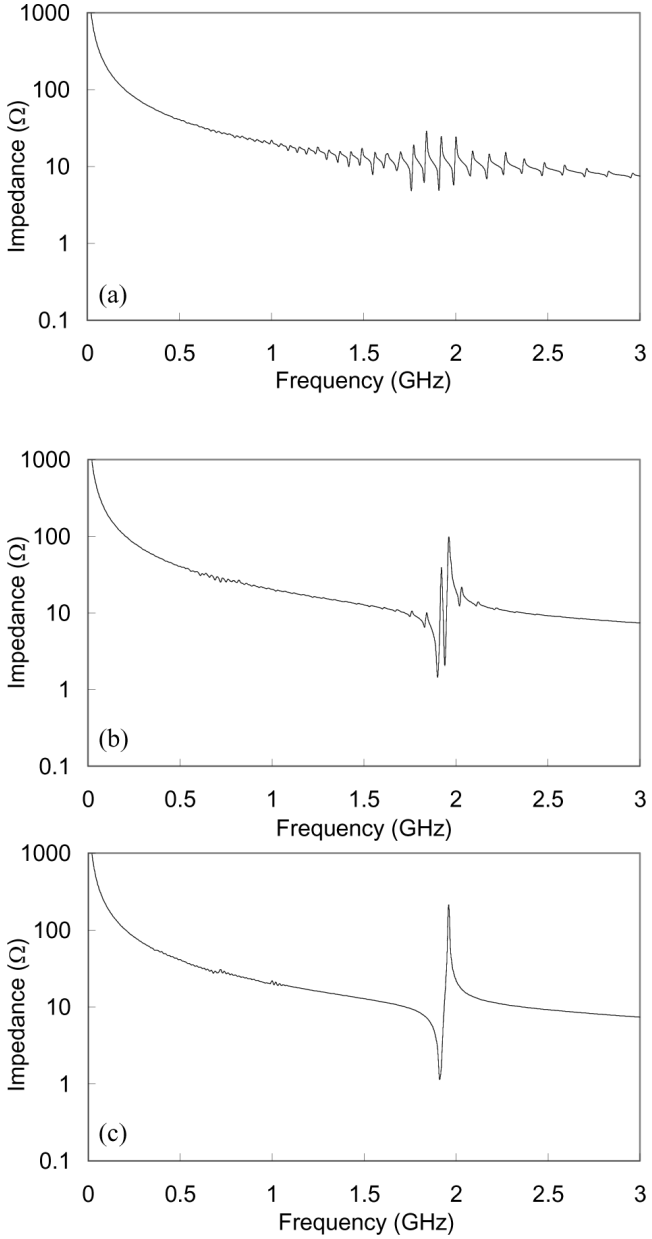

Fig. 8. Electrical input impedance frequency response of a solidly mounted acoustic wave resonator, as determined by 2D harmonic finite-element analysis. The figures show the results of simulations including (a) no pairs, (b) one pair, and (c) three pairs of acoustic reflector layers. An increasing level of acoustic isolation is achieved as the number of acoustic reflector layers is increased.

C. Columnar-SMR and Planar-SMR

The harmonic technique for determining the resonance and anti-resonance frequencies has been applied to both the columnar-SMR and planar-SMR structures, as illustrated in Fig. 3(b) and (c). ZnO was chosen as the piezoelectric material. Ten pairs of reflector layers were used; the layer thicknesses were 0.8 μm thick for both W and Mg. The simulations indicate that an optimum effective piezoelectric coupling factor of approximately 0.11 can be achieved using an aspect ratio of 0.85 for the columnar-SMR structure. Similarly, an optimum effective piezoelectric coupling factor of approximately 0.07 can be achieved using an aspect ratio of 0.9 for the planar-SMR structure, but full 3D analyses are required for accurate results. The results are very similar in form to those shown in Fig. 5, and so have been omitted here.

D. Summary

High mesh-density, 3D quarter-symmetry model modal analysis was run for each structure with an aspect ratio of 0.1 to determine an accurate prediction of the performance of each model, with ZnO being the material of choice. The results predicted a coupling for the planar-SMR of $k^2_{\text{eff}} = 0.115$ which is significantly higher than the 0.07 calculated from 2D analyses. The results for the columnar-SMR and membrane-FBAR were $k^2_{\text{eff}} = 0.085$ and $k^2_{\text{eff}} = 0.122$, respectively. The electromechanical coupling factor for a traditional planar membrane-supported FBAR was calculated as $k^2_{\text{eff}} = 0.052 \pm 0.002$ from 2D harmonic analyses, which compares with approximately 0.07 for real devices [18]. These results imply that there is a significant increase in coupling for the three nanostructured designs studied, particularly the membrane-FBAR.

The 2D finite element modelling of the electrical input impedance of the membrane-FBAR structure has been verified by comparisons to experimental data of FBARs fabricated at Cranfield University [18], and have shown reasonable agreement. The positions of the fundamental thickness resonance and anti-resonance frequencies match up very well, and the data even show the presence of regularly spaced spurious resonances. Unfortunately, these FEM results do not incorporate electrical losses due to the limitations of ANSYS version 5.7, and so result in a poor quality fit of data.

In order to create a useful bulk acoustic wave resonating device using the ideas discussed, a large array of resonating rods would need to be excited to achieve the required electrical characteristics. This presents a number of challenges for fabrication; however, the predicted increase in the resonator coupling coefficient would alone provide significant reason for proceeding, not ignoring the suppression of the problematic spurious modes. The finite element results imply a predicted increase in resonator coupling factor of ca. 40%, which it is hoped will transfer to the final NAPIER devices.

Although the implementation of rod-like arrays in piezoelectric resonators may improve performances, there are several potential disadvantages of the proposed structure. First, it would be particularly challenging to fabricate these devices as they have been described, although not impossible. Several options are available for the surface structuring of the piezoelectric layer into rods, such as e-beam lithography and subsequent reactive ion etching. A second problem that may be encountered could be increased losses due to the more complex structure proposed. These losses may be large enough that they even cancel out the advantages of employing rod-arrays.

V. Validation of Results

It is important to validate the accuracy of any data determined from numerical simulations. One way in which this can be achieved is by comparing the numerical results with well-understood analytical solutions. In the case of piezoelectric resonating structures, the resonance and anti-resonance frequencies of particular resonant modes can be used as a suitable comparison.

The fundamental resonance frequency, $f_1^{(r)}$, of a piezoelectric rod or bar-like structure of length l, operating in the length-extension mode, is obtained by the solution to the transcendental equation [13]:

$$\tan\left(\gamma\alpha^{(D)}\right) = \gamma\alpha^{(D)} / \left(k_{33}^{(l)}\right)^2, \tag{2}$$

where $\gamma = \omega l/2$, $\alpha^{(D)} = \left(\rho s_{33}^D\right)^{1/2}$, $k_{33}^{(l)} = d_{33}/\left(\varepsilon_{33}^T s_{33}^E\right)^{1/2}$, $\omega = 2\pi f_1^{(r)}$, and where all symbols have their usual meaning. The fundamental anti-resonance frequency, $f_2^{(r)}$, is governed by the simpler transcendental equation $\cos\left(\gamma\alpha^{(D)}\right) = 0$, which yields

$$f_2^{(r)} = \frac{m}{2l}\sqrt{\frac{1}{\rho s_{33}^D}}, \quad m \text{ odd}, \tag{3}$$

where all symbols have their usual meaning.

Similarly, the resonance and anti-resonance frequencies of a flat piezoelectric plate of thickness t, undergoing thickness extension, can also be calculated, and the fundamental resonance frequency, $f_1^{(p)}$, can be determined by solving the transcendental equation

$$\tan\left(\gamma\alpha^{(3)}\right) = \gamma\alpha^{(3)} / \left(k^{(3)}\right)^2, \tag{4}$$

where $\gamma = \omega t/2$, $\alpha^{(3)} = \left(\rho/\hat{c}^{(3)}\right))^{1/2}$, $\hat{c}^{(3)} = c_{33}^E + e_{33}^2/\varepsilon_{33}^S$, $k^{(3)} = e_{33}/\left(\varepsilon_{33}^S \hat{c}^{(3)}\right)^{1/2}$, $\omega = 2\pi f_1^{(p)}$, and where all symbols have their usual meaning. The fundamental anti-resonance frequency, $f_2^{(p)}$, is governed by the simpler transcendental equation $\cos\left(\gamma\alpha^{(3)}\right) = 0$, which yields

$$f_2^{(p)} = \frac{m}{2t}\sqrt{\frac{c_{33}^E + e_{33}^2/\varepsilon_{33}^S}{\rho}}, \quad m \text{ odd}, \tag{5}$$

where all symbols have their usual meaning.

TABLE II
VALIDATION OF FEM RESULTS.

Mode	Material		Target result (GHz)	FEM result (GHz)	Ratio	k_{eff} (FEM)
ROD length extension	ZnO	f_1	2.522	2.521	1.0004	0.353
		f_2	2.695	2.695	1.0000	
	AlN	f_1	5.105	5.106	0.9998	0.281
		f_2	5.320	5.321	0.9998	
	PZT	f_1	1.371	1.371	1.0000	0.721
		f_2	1.980	1.980	1.0000	
PLATE thickness extension	ZnO	f_1	3.056	3.060	0.9987	0.215
		f_2	3.129	3.133	0.9987	
	AlN	f_1	5.535	5.536	0.9998	0.222
		f_2	5.677	5.678	0.9998	
	PZT	f_1	2.169	2.171	0.9991	0.402
		f_2	2.368	2.371	0.9987	

It is pertinent to add that (2)–(5) are valid only for lossless resonators, and when the aspect ratios of the structures are sufficiently rod-like or plate-like. It should be noted that requirements of being rod-like become more stringent as the piezoelectric coupling factor increases. Additionally, the effects of massive electrodes have not been taken into account here.

The resonance and anti-resonance frequencies for the two end-point cases of the rod-like and plate-like modes of the freely suspended piezoelectric blocks were calculated by both modal and harmonic analyses. There was good agreement between the analytical and 2D FEM results for the plate modes. As the 2D FEM results for the rod modes were typically 15% different from the expected analytical results, full 3D analyses proved necessary to achieve good agreement. The FEM results of 2D plates and 3D rods are displayed together with the analytical calculation results for comparison in Table II. The results show excellent agreement between the analytical and finite-element results, with results typically less than 0.1%. The calculated electromechanical coupling factors from (1) for the finite-element analysis results are also included.

VI. CONCLUSIONS

Several structures have been considered and analyzed using 1D analytical modelling with the transmission-line equation and 2D and 3D finite-element modelling analyses. A suggested structure has been proposed for the NAPIER array, and the geometry optimized using FEM. The validity of the FEM results has been tested by comparisons with analytical end-point solutions and the comparisons have shown excellent agreement for both the rod and plate modes for ZnO, PZT, and AlN.

The results suggest that a higher coupling factor can be achieved over the standard FBAR design by implementing rod-type instead of plate-type resonance modes. The planar-SMR type structure appears not to give any noticeable advantages over the plate membrane-FBAR. However, the columnar-SMR and membrane-FBAR structures implementing the rod-like NAPIER array present significant advantages in terms of increased coupling and reduced spurious resonances. For the membrane-FBAR structures, an aspect ratio of less than 0.5 is required for all the rod-like resonating blocks in order to achieve an effective coupling of over 0.1 for ZnO piezoelectric material. Optimum performance can be achieved for rod widths < 100 nm for resonators where the piezoelectric layer is of the order 1 μm thick. For higher frequency resonators, a thinner piezoelectric layer is required, implying even tighter constraints on the widths of the rods and the need for the nanostructuring of such devices.

REFERENCES

[1] T. Gururaja, W. Schulze, L. Cross, B. Auld, Y. Shui, and Y. Wang, "Resonant modes of vibration in piezoelectric PZT-polymer composites with two dimensional periodicity," *Ferroelectrics*, vol. 54, pp. 183–186, 1984.

[2] B. Auld and J. Hossack, "Distributed-period structures for suppression of spurious modes in 1-3 piezocomposites," *Electron. Lett.*, vol. 27, no. 14, pp. 1284–1285, July 1991.

[3] W. Smith, A. Shaulov, and B. Auld, "Design of piezocomposites for ultrasonic transducers," *Ferroelectrics*, vol. 91, pp. 155–162, 1989.

[4] J. Hossack and B. Auld, "Improved efficiency piezoelectric ceramic/polymer composite transducers," in *Proc. IEEE Ultrason. Symp.*, 1992, pp. 523–526.

[5] W. Smith and B. Auld, "Modeling 1-3 composite piezoelectrics: Thickness-mode oscillations," *IEEE Trans. Ultrason., Ferroelect., Freq. Contr.*, vol. 38, no. 1, pp. 40–47, Jan. 1991.

[6] K. Lakin, G. Kline, and K. McCarron, "Development of miniature filters for wireless applications," *IEEE Trans. Microwave Theory Tech.*, vol. 43, no. 12, pp. 2933–2939, Dec. 1995.

[7] T. Makkonen, J. Koskela, and M. Salomaa, "Two-dimensional FEM model for crystal resonators," in *Proc. IEEE Ultrason. Symp.*, 1997, pp. 951–954.

[8] T. Makkonen, A. Holappa, J. Ella, and M. Salomaa, "Finite element simulations of thin-film composite BAW resonators," *IEEE Trans. Ultrason., Ferroelect., Freq. Contr.*, vol. 48, no. 5, pp. 1241–1258, Sep. 2001.

[9] P. Tikka, J. Kaitila, M. Ylilammi, T. Makkonen, J. Knuttila, K. Hashimoto, and M. Salomaa, "Laser probing and FEM modeling of ultrasonically vibrating surfaces," in *Proc. IEEE Ultrason. Symp.*, 1998, pp. 1143–1146.

[10] P. Tikka, J. Kaitila, J. Ella, T. Makkonen, J. Knuttila, J. Westerholm, and M. Salomaa, "Laser probing and FEM modeling of solidly mounted resonators," *IEEE MTT-S Int. Microwave Symp. Dig.*, vol. 3, pp. 1373–1376, 1999.

[11] H. Kunkel, S. Locke, and B. Pikeroen, "Finite-element analysis of vibrational modes in piezoelectric ceramic disks," *IEEE*

Trans. Ultrason., Ferroelect., Freq. Contr., vol. 37, no. 4, pp. 316–327, July 1990.

[12] R. Lerch, "Simulation of piezoelectric devices by two- and three-dimensional finite elements," *IEEE Trans. Ultrason., Ferroelect., Freq. Contr.*, vol. 37, no. 2, pp. 233–247, May 1990.

[13] *IEEE Standard on Piezoelectricity—ANSI/IEEE Std 176-1987*, 1988, Standards Committee of the IEEE Ultrason., Ferroelect. Freq. Contr. Soc..

[14] M. Choy, W. Cook, R. Hearmon, H. Jaffe, J. Jerphagnon, S. Kurtz, S. Liu, and D. Nelson, "Elastic, Piezoelectric, Pyroelectric, Piezooptic, Electrooptic Constants and Nonlinear Dielectric Susceptibilities of Crystals," in *Group III: Condensed Matter*. K. Hellwege and A. Hellwege, Eds. Berlin: Springer-Verlag, 1984, p. 559.

[15] S. Sherrit, H. Wiederick, and B. Mukherjee, "A complete characterization of the piezoelectric, dielectric, and elastic properties of Motorola PZT 3203 HD including losses and dispersion," in *Proc. SPIE Med. Imag. Conf.*, Newport Beach, CA, vol. 3037, Feb. 1997, pp. 158–169.

[16] K. Tsubouchi and N. Mikoshiba, "Zero-temperature-coefficient SAW devices on AlN epitaxial films," *IEEE Trans. Sonics Ultrason.*, vol. SU-3, no. 5, Sep. 1985, pp. 634–644.

[17] K. Lakin, K. McCarron, and R. Rose, "Solidly mounted resonators and filters," in *Proc. IEEE Ultrason. Symp.*, 1995, pp. 905–908.

[18] Q. Su, P. Kirby, E. Komuro, M. Imura, Q. Zhang, and R. Whatmore, "Thin-film bulk acoustic resonators and filters using ZnO and lead-zirconium-titanate thin films," *IEEE Trans. Microwave Theory Tech.*, vol. 49, no. 4, pp. 769–778, Apr. 2001.